

## Probing the nature of electroweak symmetry breaking with Higgs boson pair-production at ATLAS

---

**Michael Hank, on behalf of the ATLAS Collaboration<sup>a,\*</sup>**

<sup>a</sup>*Enrico Fermi Institute, University of Chicago,  
5640 S Ellis Ave, Chicago IL, United States of America*

*E-mail: [mhank@uchicago.edu](mailto:mhank@uchicago.edu), [michael.donald.hank@cern.ch](mailto:michael.donald.hank@cern.ch)*

The ground state of the Higgs potential is found at a non-zero value of the Higgs field. This spontaneously breaks the electroweak symmetry, generating masses for most Standard Model particles. The shape of the Higgs potential is determined by the Higgs boson self-coupling, which can be probed through the pair production of Higgs bosons. This proceeding reports results for the latest  $HH$  searches by the ATLAS experiment in the  $b\bar{b}\gamma\gamma$ ,  $b\bar{b}\tau^+\tau^-$ , and  $b\bar{b}b\bar{b}$  decay channels. These are obtained from the full LHC Run 2 dataset with  $\sqrt{s} = 13$  TeV  $pp$  collisions. Non-resonant  $HH$  results are interpreted as constraints on the Higgs boson self-coupling as well as upper limits on the Standard Model signal strength. Limits are also set on heavy resonances decaying to Higgs boson pairs.

*7th Symposium on Prospects in the Physics of Discrete Symmetries (DISCRETE 2020-2021)  
29th November - 3rd December 2021  
Bergen, Norway*

---

\*Speaker

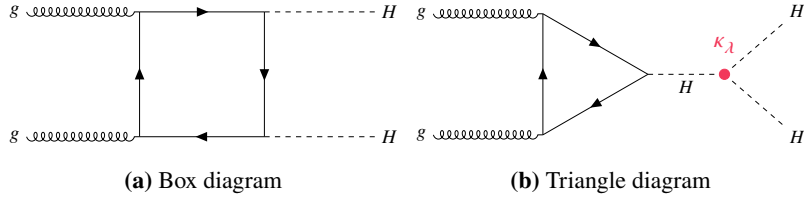


**Figure 1:** Leading-order Feynman diagrams for ggF non-resonant Higgs boson pair production [5].

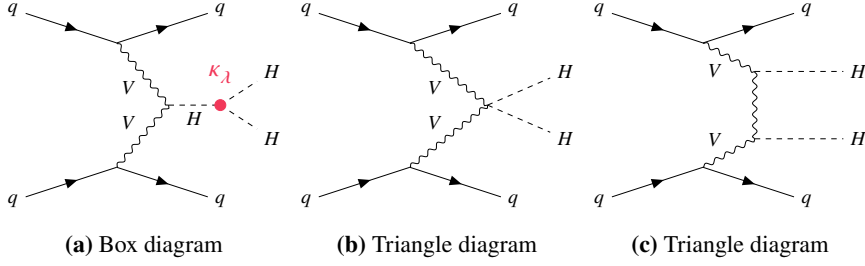


**Figure 2:** Leading-order Feynman diagrams for VBF non-resonant Higgs boson pair production [5].

## 1. Introduction

While the Higgs boson was discovered in 2012 [1, 2], the shape of the Higgs potential has not yet been measured. This shape has strong implications for electroweak symmetry breaking and models of electroweak baryogenesis [3]. The shape can be probed by the ATLAS detector [4] at the Large Hadron Collider (LHC) using pair production of Higgs bosons. Searches are performed for various channels using up to  $139 \text{ fb}^{-1}$  of data.

The primary production mechanism for non-resonant Higgs boson pair production is gluon fusion (ggF). This occurs through two leading-order diagrams, the box diagram and the triangle diagram, shown in Figure 1. These diagrams interfere destructively, leading to a production cross section of  $\sigma_{\text{ggF}}^{\text{SM}} = 31.05 \text{ fb}$  at 13 TeV with the Higgs mass set to  $m_H = 125 \text{ GeV}$  [5]. The secondary production mode, vector boson fusion (VBF), has a roughly 5% contribution to  $\sigma_{HH}^{\text{SM}}$  (see Figure 2). This corresponds to  $\sigma_{\text{VBF}}^{\text{SM}} = 1.73 \text{ fb}$  (at 13 TeV with  $m_H = 125 \text{ GeV}$ ) [5].

Both the ggF and VBF production modes are sensitive to  $\kappa_\lambda = \lambda_{HHH}/\lambda_{HHH}^{\text{SM}}$ , the ratio of the trilinear Higgs self-coupling to the Standard Model (SM) value. As  $\kappa_\lambda$  diverges from the SM value, the cross section of Higgs boson pair production can increase by orders of magnitude [6]. While the SM cross section is too small to be observed at ATLAS with the current dataset, it could be possible to observe or exclude some non-SM values with larger cross sections. Searches are presented for the ggF and VBF production modes in the  $b\bar{b}\gamma\gamma$  and  $b\bar{b}\tau^+\tau^-$  decay channels.

In order to change  $\kappa_\lambda$  while retaining gauge invariance and renormalizability, it is necessary to introduce other new physics. One possible mechanism is to introduce a resonance that decays to pairs of Higgs bosons. Two models are investigated: a spin-0 resonance  $X$  (see Figure 3), which occurs in models such as the two-Higgs-doublet model (2HDM) [7], and a spin-2 Kaluza-Klein graviton in the context of the bulk Randall-Sundrum model [8]. Searches are presented for the  $b\bar{b}\gamma\gamma$ ,  $b\bar{b}\tau^+\tau^-$ , and  $b\bar{b}b\bar{b}$  decay channels.

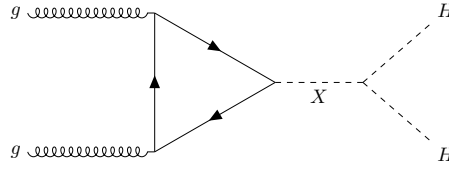


**Figure 3:** Leading-order Feynman diagram for Higgs boson pair production via a scalar resonance  $X$  [5].

## 2. Non-Resonant Searches

### 2.1 $b\bar{b}\gamma\gamma$

As the photon does not couple directly to the Higgs boson, the  $H \rightarrow \gamma\gamma$  decay must proceed via loops. This leads to a  $HH \rightarrow b\bar{b}\gamma\gamma$  branching ratio of only 0.26%. Despite this, the signature is cleaner than other decay modes, allowing it to compete with higher branching ratio channels.

The  $b\bar{b}\gamma\gamma$  analysis [9] searches for events with two  $b$ -jets and two photons. A combined strategy is used to target both the ggF and VBF channels. Events are selected using di-photon triggers. The primary background is  $\gamma\gamma$ +jets. This is estimated using a functional form derived by fitting on a high-statistics MC background template. A corrected invariant mass,  $m_{b\bar{b}\gamma\gamma}^* = m_{b\bar{b}\gamma\gamma} - m_{b\bar{b}} - m_{\gamma\gamma} + 250$  GeV, is used to separate events into a low-mass ( $m_{b\bar{b}\gamma\gamma}^* < 350$  GeV) and high-mass ( $m_{b\bar{b}\gamma\gamma}^* > 350$  GeV) category. In each category, a Boosted Decision Tree (BDT) is used to discriminate between signal ( $\kappa_\lambda = 10$  for low-mass, 1 for high-mass) and background events. Two signal regions are created for each category: a tight region using the events with BDT scores closest to 1, and a loose region using events with slightly lower BDT scores. The final results are then obtained by fitting  $m_{\gamma\gamma}$  between 105 and 160 GeV.

This analysis constrains the signal strength to be  $< 4.2$  times the SM value (5.7 expected). These limits are approximately 5 times stronger than the previous  $36.1 \text{ fb}^{-1}$  results [10]. In terms of  $\kappa_\lambda$ , 95% confidence level (CL) upper limits exclude the region outside  $-1.5 < \kappa_\lambda < 6.7$  ( $-2.4 < \kappa_\lambda < 7.7$  expected).

### 2.2 $b\bar{b}\tau^+\tau^-$

The  $HH \rightarrow b\bar{b}\tau^+\tau^-$  analysis [11] searches for events with 2  $b$ -jets and 2  $\tau$ -leptons. This channel has a branching ratio of 7.3%. The ggF and VBF channels are targeted using a combined strategy. Events are split into three categories. The first category contains all-hadronic events where each  $\tau$  candidate decays hadronically. The second and third categories contain semi-leptonic events where one  $\tau$  decays hadronically and the other decays leptonically and which pass either a single-lepton or a lepton-plus- $\tau$  trigger respectively. The largest backgrounds are  $t\bar{t}$  and  $Z$  + heavy flavor. These and smaller backgrounds are estimated using a combination of MC and data-driven techniques, where the latter are used to estimate the contributions from fake hadronic  $\tau$  candidates. The signal is then extracted using a BDT for the all-hadronic channel and neural networks (NNs) for the semi-leptonic channels. A fit on the outputs of these multivariate discriminants (MVs) is used to obtain the results.

The signal strength is constrained at 95% CL to be less than 4.7 times the SM value (3.9 expected). These limits are 2.7 (3.8) times stronger than the previous limits with  $36.1 \text{ fb}^{-1}$  [12].  $\kappa_\lambda$  is constrained to fall between -2.4 and 9.2 (-2.0 to 9.0 expected) [5].

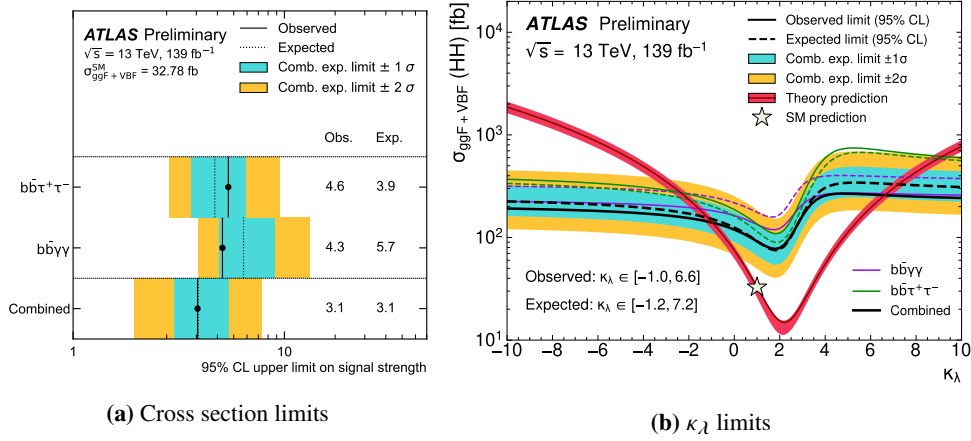


**Figure 4:** Upper limits on di-Higgs production for the non-resonant analyses [5].

## 2.3 Combination

The results from the  $b\bar{b}\gamma\gamma$  and  $b\bar{b}\tau^+\tau^-$  channels are combined [5]. The orthogonality of the analyses is checked, and the systematics are correlated where possible. Minor updates are made to the Higgs boson mass value used in the  $b\bar{b}\gamma\gamma$  analysis.

Cross sections above 3.1 times the SM (3.1 expected) are excluded at 95% CL (Figure 4a). Though this result has fewer channels, it improves on the  $36.1 \text{ fb}^{-1}$  results by a factor of 2.2 (3.2 expected) [13]. As shown in Figure 4b,  $\kappa_\lambda$  is constrained to fall between -1.0 and 6.6 (-1.2 to 7.2 expected). These are the strongest limits on the SM cross section and  $\kappa_\lambda$  to date.

## 3. Resonant Searches

### 3.1 $b\bar{b}\gamma\gamma$

Like the non-resonant analysis, the resonant  $b\bar{b}\gamma\gamma$  analysis searches for events with two  $b$ -jets and two photons [9]. Two BDTs are used to distinguish signal from background: one for  $\gamma\gamma$  background processes and one for single Higgs background processes. For each simulated resonance mass, a signal region is then constructed where  $m_{b\bar{b}\gamma\gamma}^*$  is required to be within  $2\sigma$  of the simulated signal mean for resonance masses  $m_X < 900 \text{ GeV}$  or within  $4\sigma$  for resonance masses  $m_X \geq 900 \text{ GeV}$ . The final results are obtained by fitting  $m_{\gamma\gamma}$  between 105 and 160 GeV.

### 3.2 $b\bar{b}\tau^+\tau^-$

The resonant  $b\bar{b}\tau^+\tau^-$  analysis uses a similar strategy to the non-resonant analysis [11]. The key difference is that the signal extraction uses a parameterized NN parameterized in terms of the resonance mass. The all-hadronic channel contributes most of the sensitivity for low resonance masses. A broad excess was observed between 700 GeV and 1200 GeV. This was largest at 1.0 TeV and had a  $3.0\sigma$  local,  $2.0\sigma$  global significance.

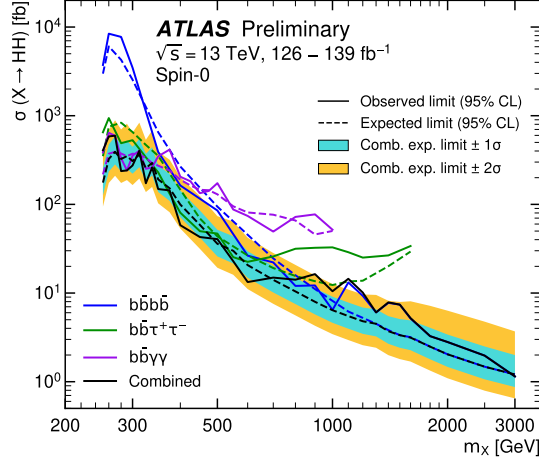


**Figure 5:** Upper limits on the di-Higgs production cross section for the resonant analyses [5].

### 3.3 $b\bar{b}b\bar{b}$

The  $HH \rightarrow b\bar{b}b\bar{b}$  analysis [14] is only used for the resonant results. This analysis has the highest branching ratio of  $HH$  decays (33.9%), but also has the largest background. There are two channels in this analysis. The first channel, resolved, searches for events with 4 small-radius ( $R=0.4$ )  $b$ -jets. The second channel, boosted, looks at events with 2 large-radius ( $R=1.0$ ) jets, containing a total of 2 to 4  $b$ -tagged track jets. Events are split into control, validation, and signal regions using the reconstructed masses of the Higgs boson candidates.

The background is mainly QCD multijet and is estimated using data-driven techniques. The kinematics of the fully-tagged regions are estimated by reweighting events from corresponding regions with fewer  $b$ -tagged jets. This is achieved using a NN for the resolved channel and splines for the boosted channel.

The results are obtained by a fit to  $m_{HH}$  after re-scaling the four-momenta of the Higgs boson candidates such that their masses are 125 GeV. A small excess is observed for a scalar resonance mass of 1.1 TeV, with  $2.5\sigma$  local and  $0.8\sigma$  global significance. For spin-2 Kaluza-Klein graviton models, gravitons with masses between 298 GeV and 1460 GeV (304 GeV to 1740 GeV expected) are excluded at 95% CL.

### 3.4 Combination

The resonant results for the  $b\bar{b}\gamma\gamma$ ,  $b\bar{b}\tau^+\tau^-$ , and  $b\bar{b}b\bar{b}$  channels are statistically combined [5]. Results are shown in Figure 5. The  $b\bar{b}\gamma\gamma$  provides the strongest constraints for scalar masses below 400 GeV. The  $b\bar{b}\tau^+\tau^-$  channel is the most sensitive between 400 GeV and 800 GeV. Finally, the  $b\bar{b}b\bar{b}$  channel provides the most stringent limits above 800 GeV.

An excess is observed at a resonance mass of  $m_X = 1100$  GeV. This was measured to have a local significance of  $3.2\sigma$  and a global significance of  $2.1\sigma$ .

## 4. Summary

Searches have been performed for resonant and non-resonant Higgs boson pair production using the ATLAS detector at the LHC. Results for the  $b\bar{b}\gamma\gamma$ ,  $b\bar{b}\tau^+\tau^-$ ,  $b\bar{b}b\bar{b}$  (resonant-only) and combined decay channels are presented.

The results of the non-resonant analyses set the strongest limits to date on the trilinear Higgs boson self-coupling, parameterized in terms of  $\kappa_\lambda$ . At 95% confidence level,  $\kappa_\lambda$  is constrained to fall between -1.0 and 6.6 (-1.2 and 7.2 expected). Despite containing fewer channels, this is significantly improved over previous results with  $36.1 \text{ fb}^{-1}$  of data [13]. The resonant analyses set strong limits on the cross section of heavy scalars decaying to pairs of Higgs bosons. In addition, the  $b\bar{b}b\bar{b}$  is used to constrain the production of spin-2 Kaluza-Klein gravitons, excluding masses between 298 and 1460 GeV (304 to 1740 GeV expected).

## References

- [1] ATLAS Collaboration, *Observation of a new particle in the search for the Standard Model Higgs boson with the ATLAS detector at the LHC*, *Phys. Lett. B* **716** (2012) 1 [hep-ex/1207.7214].
- [2] CMS Collaboration, *Observation of a new boson at a mass of 125 GeV with the CMS experiment at the LHC*, *Phys. Lett. B* **716** (2012) 30 [hep-ex/1207.7235].
- [3] A. Noble and M. Perelstein, *Higgs self-coupling as a probe of electroweak phase transition*, *Phys. Rev. D* **78** (2008) 063518 [hep-ph/0711.3018].
- [4] ATLAS Collaboration, *The ATLAS Experiment at the CERN Large Hadron Collider*, *JINST* **3** (2008) S08003.
- [5] ATLAS Collaboration, *Combination of searches for non-resonant and resonant Higgs boson pair production in the  $b\bar{b}\gamma\gamma$ ,  $b\bar{b}\tau^+\tau^-$  and  $b\bar{b}b\bar{b}$  decay channels using  $pp$  collisions at  $\sqrt{s} = 13 \text{ TeV}$  with the ATLAS detector*, ATLAS-CONF-2021-052, <https://cds.cern.ch/record/2786865>.
- [6] J. Baglio et al.,  *$gg \rightarrow HH$  : Combined uncertainties*, *Phys. Rev. D* **103** (2021) no.5, 056002 [hep-ph/2008.11626].
- [7] G. Branco et al., *Theory and phenomenology of two-Higgs-doublet models*, *Phys. Rept.* **516** (2012) 1 [hep-ph/1106.0034].
- [8] L. Randall and R. Sundrum, *Large Mass Hierarchy from a Small Extra Dimension*, *Phys. Rev. Lett.* **83** (1999) 3370 [hep-ph/9905221].
- [9] ATLAS Collaboration, *Search for Higgs boson pair production in the two bottom quarks plus two photons final state in  $pp$  collisions at  $\sqrt{s} = 13 \text{ TeV}$  with the ATLAS detector*, submitted to PRD [hep-ex/2112.11876].
- [10] ATLAS Collaboration, *Search for Higgs boson pair production in the  $\gamma\gamma b\bar{b}$  final state with 13 TeV  $pp$  collision data collected by the ATLAS experiment*, *JHEP* **11** (2018) 40 [hep-ex/1807.04873].

- [11] ATLAS Collaboration, *Search for resonant and non-resonant Higgs boson pair production in the  $b\bar{b}\tau^+\tau^-$  decay channel using 13 TeV  $pp$  collision data from the ATLAS detector*, ATLAS-CONF-2021-030, <https://cds.cern.ch/record/2777236>.
- [12] ATLAS Collaboration, *Search for resonant and non-resonant Higgs boson pair production in the  $b\bar{b}\tau^+\tau^-$  decay channel in  $pp$  collisions at  $\sqrt{s} = 13$  TeV with the ATLAS detector*, *Phys. Rev. Lett.* **121** (2018) 191801 [hep-ex/1808.00336], Erratum: *Phys. Rev. Lett.* **122** (2019) 089901.
- [13] ATLAS Collaboration, *Combination of searches for Higgs boson pairs in  $pp$  collisions at  $\sqrt{s} = 13$  TeV with the ATLAS detector*, *Phys. Lett. B* **800** (2020) 135103 [hep-ex/1906.02025].
- [14] ATLAS Collaboration, *Search for resonant pair production of Higgs bosons in the  $b\bar{b}b\bar{b}$  final state using  $pp$  collisions at  $\sqrt{s} = 13$  TeV with the ATLAS detector*, submitted to *Phys. Rev. D* [hep-ex/2202.07288].